



# Monodisperse bismuth nanoparticles decorated graphitic carbon nitride: Enhanced visible-light-response photocatalytic NO removal and reaction pathway

Guangming Jiang<sup>a</sup>, Xinwei Li<sup>a</sup>, Mengna Lan<sup>a</sup>, Ting Shen<sup>a</sup>, Xiaoshu Lv<sup>a</sup>, Fan Dong<sup>a,\*</sup>, Sen Zhang<sup>b,\*</sup>

<sup>a</sup> Engineering Research Center for Waste Oil Recovery Technology and Equipment, Ministry of Education, Chongqing Key Laboratory of Catalysis and Functional Organic Molecules, Chongqing Technology and Business University, Chongqing 400067, China

<sup>b</sup> Department of Chemistry, University of Virginia, Charlottesville, VA 22904, United States

## ARTICLE INFO

### Article history:

Received 2 October 2016

Received in revised form

15 December 2016

Accepted 3 January 2017

Available online 4 January 2017

### Keywords:

Photocatalysis

Surface plasmon resonance

Heterojunction

Bismuth

NO removal

## ABSTRACT

We report a facile approach to monodisperse bismuth nanoparticles (Bi NPs)-decorated graphitic carbon nitride ( $\text{g-C}_3\text{N}_4$ ) photocatalyst, and its high efficiency in removing ppb-level NO in a continuous gas flow under visible light illumination. The photocatalyst is prepared via a size-controllable synthesis of Bi NPs in organic colloidal solution and a subsequent assembly of them on  $\text{g-C}_3\text{N}_4$ . The incorporation of Bi NPs can significantly enhance the photocatalytic activity of  $\text{g-C}_3\text{N}_4$  via the construction of Bi- $\text{g-C}_3\text{N}_4$  heterojunction (heterojunction effect) and their surface plasmon resonance effect (SPR effect), both of which can promote the separation of photoexcited electron/hole in  $\text{g-C}_3\text{N}_4$ . Furthermore, tuning the size of Bi NPs allows the precise control of the heterojunction density and the intensity of SPR, and thus the successful identification and optimization of the contribution of each effect to the photocatalysis. 12 nm Bi NPs-decorated  $\text{g-C}_3\text{N}_4$  can achieve an exceptional NO removal efficiency of 60.8%, much higher than those of smaller or larger Bi NPs decorated  $\text{g-C}_3\text{N}_4$  and the bare  $\text{g-C}_3\text{N}_4$  (38.6%) under the same condition. This work highlights a NP size-controlled strategy to tuning the synergistic heterojunction and SPR effect in metal NPs-semiconductor photocatalysis, which could be generalized in designing efficient and cost-effective photocatalytic systems for the clean-up of many other atmospheric pollutants.

© 2017 Elsevier B.V. All rights reserved.

## 1. Introduction

The increasing awareness of environmental and health concerns have motivated the enormous efforts in developing efficient and cost-effective technologies to detect, regulate and remove the various atmospheric gas pollutants, including nitric oxide ( $\text{NO}_x$ ), sulfur oxide ( $\text{SO}_x$ ), volatile organic compounds (VOC) and particle matters (PM). Among them, NO is deemed as a critical threat to human health and global climate, as it is the paramount contributor to the formation of hazardous acid rain, haze and photochemical smog, etc [1,2]. Several approaches, including physical/chemical adsorption [3], heterogeneous catalytic reduction [4] and oxidation [5], have been reported to show high efficiency in selective sequestration and conversion of NO. But these methods are always studied for treatment of atmospheric NO with a relatively high concentration,

and become capital and energy prohibitive in clean-up of ppb-level NO. For the practical ppb-level NO treatment, it is highly desirable, but still challenging, to develop an approach with the features of: (i) high NO conversion efficiency at room temperature, (ii) stable performance for large-scale gas cleaning and (iii) sustainable and low-cost energy input.

Herein, we report a unique photocatalytic approach, based on monodisperse bismuth nanoparticles (Bi NPs)-decorated graphitic carbon nitride ( $\text{g-C}_3\text{N}_4$ ) photocatalyst, to reach the aforementioned requirements and allow the efficient ppb-level NO removal in a continuous air flow under visible light illumination. Among the various photocatalyst choices (such as  $\text{TiO}_2$  [6,7],  $\text{CdS}$  [8], W- and Bi-based salts [9,10] etc.), we specifically focus on  $\text{g-C}_3\text{N}_4$  which has a band gap of 2.69 eV and a proper position of conduction/valance band [11,12]. The former characteristic enable  $\text{g-C}_3\text{N}_4$  to generate excited electron/hole ( $e^-/h^+$ ) pairs under visible light illumination, while the latter one endows  $h^+$  and  $e^-$  with high power to oxidize NO in either a direct pathway ( $h^+$  oxidizes NO) or an indirect pathway ( $e^-$  can trigger the generation of oxidative radicals for

\* Corresponding authors.

E-mail addresses: [dfctbu@126.com](mailto:dfctbu@126.com) (F. Dong), [sz3t@virginia.edu](mailto:sz3t@virginia.edu) (S. Zhang).

NO oxidation) [13,14]. In addition, the facile preparation of g-C<sub>3</sub>N<sub>4</sub> and its rich earth-abundance further make it highly suitable for large-scale application [15,16]. But we notice that the bare g-C<sub>3</sub>N<sub>4</sub> is not active enough for NO conversion, which could be ascribed to the fast recombination of photoexcited e<sup>-</sup>/h<sup>+</sup> pairs [17]. Our previous report has also shown that the *in-situ* formation of Bi NPs (polydisperse NPs) on g-C<sub>3</sub>N<sub>4</sub> could increase the removal efficiency, possibly due to the surface plasmon resonance (SPR) and Bi-g-C<sub>3</sub>N<sub>4</sub> heterojunction-induced enhancement for e<sup>-</sup>/h<sup>+</sup> separation [18]. To systematically study the synergistic interaction between Bi NPs and g-C<sub>3</sub>N<sub>4</sub>, we use monodisperse Bi NPs with tunable size to precisely control their SPR intensity and the density of Bi-g-C<sub>3</sub>N<sub>4</sub> heterojunctions, which allow the identification and optimization of the contribution of each effect to the photocatalysis. With a Bi loading of 11.8 wt%, 12 nm is found to be the nearly optimal size that could maximize the synergistic contribution of SPR and heterojunction effect with Bi/g-C<sub>3</sub>N<sub>4</sub>-12 showing an exceptional NO removal efficiency of 60.8%, higher than those of smaller and larger Bi NPs decorated g-C<sub>3</sub>N<sub>4</sub> and bare g-C<sub>3</sub>N<sub>4</sub> (38.6%). The photocatalytic reaction pathway is also investigated via the identification of the active species on catalyst surface and *in situ* characterization of the intermediate product evolution during NO oxidation. The present study provides a general strategy to design and fabrication of efficient photocatalyst for ppb-level gas pollutant treatment.

## 2. Materials and methods

### 2.1. Materials

Bismuth neodecanoate, tri-*n*-octylphosphine (TOP), 1,2,3,4-tetrahydronaphthalene (tetralin, >97%) and 1-dodecanethiol were purchased from Sigma-Aldrich. Hexane, anhydrous ethanol, acetone and anhydrous hydrazine were purchased from Sinopharm Chemical Reagent Co., Ltd., Shanghai, China. All chemicals were used without further purification.

### 2.2. Synthesis of Bi NPs

Bi NPs were synthesized by modifying a previously reported method [19]. Typically, 1.0 mmol of bismuth neodecanoate were dissolved in 12 mL of tetralin, which were magnetically stirred at 110 °C under N<sub>2</sub> flow for 30 min to remove the dissolved oxygen and moisture. After cooling to 80 °C, 0.24 mL of dodecanethiol and 1.5 mL of TOP were injected into the mixture in sequence, leading to a color change in solution from transparent to yellow, brown and black. The yellow color arises from the formation of bismuth-dodecanethiol complex, which could be easily reduced into Bi NPs by TOP. The brown color indicates the formation of Bi NPs. After TOP addition, the mixture was cooled to and aged at 65 °C for another 30 mins for the growth of Bi NPs. Once cooled to room temperature, Bi NPs were collected by adding ethanol and centrifugation (5500 rpm, 3 mins), and further purified with hexane/ethanol and redispersed in hexane for future usage. Such an approach yields 12 nm Bi NPs. Different from Son et al's work [19], tetralin was chosen to substitute 1-octadecene as the solvent, which was proved to be critical to obtain well-dispersible Bi NPs in hexane. Under the same condition and when 1.0 and 2.0 mL of TOP were injected, 7 and 20 nm Bi NPs could be synthesized respectively. With the aging temperature increasing to 70 and 75 °C and the aging time decreasing to 5 mins, the Bi NP size could be controlled to be 50 and 80 nm, respectively.

### 2.3. Catalyst preparation

The as-synthesized Bi NPs and g-C<sub>3</sub>N<sub>4</sub> (0.20 g, g-C<sub>3</sub>N<sub>4</sub> was synthesized following our previous work [20]) in a certain mass ratio

were mixed in 30 mL hexane, and sonicated for 1.0 h to deposit NPs on g-C<sub>3</sub>N<sub>4</sub>. The Bi/g-C<sub>3</sub>N<sub>4</sub> composites were separated by centrifugation (5000 rpm, 3 mins) and then dried at ambient condition. The collected powder was added into an anhydrous hydrazine ethanol solution (15 vol% hydrazine) and kept stirring overnight to remove the surfactant, which was then collected by centrifugation and washed by ethanol several times to remove the residue hydrazine. The collected Bi/g-C<sub>3</sub>N<sub>4</sub> was further annealed at 180 °C for 1.0 h under a forming gas (4% H<sub>2</sub> + Ar) flow. Once cooled down, the product was stored and protected from light for further usage.

### 2.4. Photocatalytic activity evaluation on ppb-level NO removal under visible light illumination

The photocatalytic activity was evaluated by measuring its efficiency for ppb-level NO removal in a continuous flow reactor at room temperature. The rectangular reactor, made of stainless steel and covered with Saint-Glass, has a volume capacity of 4.5 L (30 cm × 15 cm × 10 cm). A 150 W commercial tungsten halogen lamp is vertically placed on top of the reactor, and the UV-light part is removed by adopting a UV cutoff filter (420 nm). The photocatalyst (0.2 g) was dispersed into 15 mL of ethanol via the sonication and then painted onto the bottom of two culture dishes (made of glass, 12.0 cm in diameter,). Then, the dishes are vacuum dried and placed at the center of the reactor. NO gas is supplied by a compressed gas cylinder with a concentration of 100 ppm (N<sub>2</sub> balance), which is further diluted to 500 ppb by the air stream. The desired relative humidity level in NO flow was controlled at 50% by passing the zero air streams through a humidification chamber. A gas blower premixed the gas streams completely, and a mass flow controller was used to control the flow rate at 2.4 L min<sup>-1</sup>. The lamp was turned on once the adsorption-desorption equilibrium was achieved. One chemiluminescence NO analyzer (Thermo Environmental Instruments Inc., 42i-TL) continuously measured the NO concentration at a sampling rate of 1.0 L min<sup>-1</sup>. The removal efficiency ( $\eta$ ) was calculated as  $\eta (\%) = (1 - C/C_0) \times 100\%$ , where C and C<sub>0</sub> are the NO concentrations in the outlet and feeding stream, respectively.

### 2.5. Characterization

Transmission electron microscopy (TEM) and High-Resolution TEM (HRTEM) images were obtained on JEOL, JEM-2010 operated at 200 kV. The sample was prepared by depositing a single drop of diluted NPs or powder dispersion on an amorphous carbon coated copper grid. X-ray diffraction (XRD, D/max RA) characterization was carried out on an X-ray diffractometer equipped with Cu K $\alpha$  radiation. X-ray photoelectron spectroscopy (XPS) were obtained on Thermo ESCALAB 250 at 150 W under Al K $\alpha$  X-rays ( $h\nu = 1486.6$  eV) radiation. Photoluminescence spectra were measured by a fluorescence spectrophotometer (F-7000) using a Xe lamp as the excitation source with optical filters. For Fourier Transform Infrared Spectroscopy (FTIR, IRAffinity-1) analysis, thin films of ground sample and KBr were prepared and the spectra were collected at 4 cm<sup>-1</sup> resolution over the frequency of 500–4000 cm<sup>-1</sup>. UV-vis Diffuse Reflection Spectra (UV-vis DRS) were obtained on a Scan UV-vis spectrophotometer (UV-2450) equipped with an integrating sphere assembly and 100% BaSO<sub>4</sub> as the reflectance sample. One spectrometer (JES FA200) was used to record the Electron Spin Resonance (ESR) signals of the radical ·OH and ·O<sub>2</sub><sup>-</sup>, and the sample was prepared by dispersing the photocatalyst into a 40 mM DMPO solution tank (aqueous dispersion for ·OH trapping and methanol dispersion for ·O<sub>2</sub><sup>-</sup> trapping). The surface photovoltage (SPV) measurements were conducted on home-built apparatus equipped with a lock-in amplifier (SR830) synchronized with a light chopper (SR540). *In situ* Diffuse Reflectance Infrared Fourier

Transform Spectroscopy (DRIFTS) measurement was conducted on a TENSO II FTIR spectrometer (Bruker) equipped with an *in situ* Diffuse- Reflectance cell (Harrick), and the sample pretreatment and the measurement procedure follow Zhou's work [21].

### 3. Results and discussions

#### 3.1. Preparation of Bi NP-decorated $g\text{-C}_3\text{N}_4$ for photocatalytic NO removal

**Fig. 1a** is a typical TEM image of the as-synthesized Bi NPs, which demonstrates the NPs' high uniformity in size (diameter:  $12.0 \pm 0.5$  nm) and morphology (spherical). The NPs are stabilized by dodecanethiol, which prevent NPs from the aggregation and make them well-dispersible in hexane (Fig. S1). A representative HRTEM image is shown in **Fig. 1b**, in which two adjacent Bi NPs display a core/shell structure with a clear interface between core and shell. The core region possesses a crystal lattice spacing of 0.328 nm, corresponding to (012) interplanar distance of rhombohedral-phase Bi. In contrast, 1.2 nm thick shell region is amorphous, as it presents no detectable crystallographic periodicity. Considering Bi is prone to be oxidized once exposed to air, even at room temperature, the shell material should be amorphous bismuth oxide ( $\text{BiO}_x$ ) [22]. The XRD pattern of the NP sample in **Fig. 1c** indicates the formation of pure rhombohedral-phase Bi (JSPDS PDF card 44-1246) by the characteristic diffraction peaks of (012), (104), (110), (015), (113), (024) and (122).  $\text{BiO}_x$  shell phase is not detected due to its amorphous nature. We notice that  $\text{BiO}_x$  shell can prevent Bi core from further oxidation, since the XRD pattern of these Bi NPs after exposed to air for one month appears the same with that of the as-synthesized Bi NPs, similar to many other air-sensitive metallic NPs [23]. As previously reported [24], Bi has a unique SPR property, which can be characterized by its UV-vis absorption spectra in the wavelength range of 300–800 nm. As clearly seen in **Fig. 1d**, the as-synthesized 12 nm Bi NPs display a broad and strong absorption ranging from 300 to 800 nm with two peaks at 390 and 565 nm, which is different to that of the bismuth-dodecanethiol complex (Denoted as  $\text{RSH}\text{-Bi}^{3+}$ ) with only a sharp absorption existing at 360 nm. It further confirms that metallic Bi NPs are produced and their plasmonic absorption band still falls into the visible light range in the presence of amorphous  $\text{BiO}_x$  surface shell.

These 12 nm Bi NPs were loaded onto  $g\text{-C}_3\text{N}_4$  under the assistance of an intense sonication to ensure that Bi NPs could be uniformly distributed on  $g\text{-C}_3\text{N}_4$ , and the resultant composite (denoted as  $\text{Bi/g-C}_3\text{N}_4\text{-12}$ ) was used for visible-light-response photocatalytic removal of ppb-level NO in a continuous air flow. Since Bi NPs are surrounded by the bulky dodecanethiol (surfactant) which may block the direct contact between Bi NPs and  $g\text{-C}_3\text{N}_4$  and hinder the electron/mass transfer among Bi NPs,  $g\text{-C}_3\text{N}_4$  and the reactants, a combined post-treatment of hydrazine washing and thermal annealing under a reductive atmosphere is employed to remove the surfactant on  $\text{Bi/g-C}_3\text{N}_4$ . The hydrazine could replace the surfactant through a ligand-exchange process [22], while the subsequent thermal annealing treatment will promote the contact of Bi NPs and  $g\text{-C}_3\text{N}_4$ , facilitating the electron transfer between them [25]. **Fig. 2a** presents a TEM image of the treated  $\text{Bi/g-C}_3\text{N}_4\text{-12}$  (denoted as  $\text{Bi/g-C}_3\text{N}_4\text{-HA-12}$ ), which indicates that Bi NPs are uniformly distributed on  $g\text{-C}_3\text{N}_4$  (TEM image with a lower magnification can be found in Fig. S2), and the treatment process show a negligible effect on the shape/size of Bi NPs. The Bi content in  $\text{Bi/C}_3\text{N}_4\text{-HA-12}$  is around 11.8 wt% determined by ICP analysis. The FTIR spectra of Bi NPs before and after hydrazine washing are exhibited in Fig. S3a, and the apparent decrease in the peak intensity of C-S vibrating absorption demonstrates the high efficiency of hydrazine washing to remove surfactant. Besides, XPS analy-

ses on  $\text{Bi/g-C}_3\text{N}_4\text{-12}$  and  $\text{Bi/g-C}_3\text{N}_4\text{-HA-12}$  suggest that the atomic percentage of sulfur (from dodecanethiol) in  $\text{Bi/g-C}_3\text{N}_4\text{-HA-12}$  is significantly reduced, further confirming that most of the surfactants have been removed (See Fig. S3). It should be noted that the hydrazine is a reductant, which should convert the surface  $\text{BiO}_x$  to the metallic in principle. However, the XPS result in Fig. S3 shows that the atomic percentage of oxygen and the intensity of Bi-O bond are still very high. This is because the reduced Bi can be easily re-oxidized at ambient condition.

**Fig. 2b** presents the photocatalytic activities of Bi NPs,  $g\text{-C}_3\text{N}_4$ ,  $\text{Bi/g-C}_3\text{N}_4\text{-12}$ ,  $\text{Bi/g-C}_3\text{N}_4\text{-H-12}$  (the sample after hydrazine washing but without the treatment of thermal-annealing) and  $\text{Bi/g-C}_3\text{N}_4\text{-HA-12}$ , which were evaluated by the ratio of NO concentration in outlet streams ( $C$ ) to that in feeding streams ( $C_0$ ). It is observed that all  $\text{Bi/g-C}_3\text{N}_4\text{-12}$  composites show much higher NO removal efficiencies [calculated by  $(1-C/C_0) \times 100\%$ ] than both the non-active Bi NPs (2.15%) and  $g\text{-C}_3\text{N}_4$  (38.6%) as well as their sum (40.75%), clearly proving the promoting role of Bi NPs on photocatalytic performance of  $g\text{-C}_3\text{N}_4$ . Among them,  $\text{Bi/g-C}_3\text{N}_4\text{-HA-12}$  acts the best with a NO removal efficiency of 60.8%, followed by  $\text{Bi/g-C}_3\text{N}_4\text{-H-12}$  (56.7%) and  $\text{Bi/g-C}_3\text{N}_4\text{-12}$  (46.7%), suggesting the importance of post-treatment on NO removal efficiency. The durability of  $\text{Bi/g-C}_3\text{N}_4\text{-HA-12}$  was tested under the repeated light on/off conditions plus a long-term light illumination, and then compared to that of  $g\text{-C}_3\text{N}_4$ . **Fig. 2c** shows that both  $\text{Bi/g-C}_3\text{N}_4\text{-HA-12}$  and  $g\text{-C}_3\text{N}_4$  could remain their NO removal efficiencies after the fifth repeated on/off and a long-term illumination (total 600 min), but  $\text{Bi/g-C}_3\text{N}_4\text{-HA-12}$  preserved its much higher efficiency over  $g\text{-C}_3\text{N}_4$ . The structure and morphology of  $\text{Bi/C}_3\text{N}_4\text{-HA-12}$  before and after the durability test were also monitored, as presented in Figs. 2 d and S4. The almost unchanged diffraction peaks of both  $g\text{-C}_3\text{N}_4$  and Bi phases in XRD patterns, as well as the well-maintained dispersity and shape of Bi NPs confirm that  $\text{Bi/g-C}_3\text{N}_4\text{-HA-12}$  photocatalyst has a high resistance to the various deactivating factors (photocorrosion and poisoning, etc.).

#### 3.2. Role of Bi NPs

The  $e^-/h^+$  separation efficiency is an excellent descriptor for the performance of a photocatalyst, and higher separation efficiency usually yields a higher activity. Therefore, to explore the role of Bi NPs,  $e^-/h^+$  separation efficiencies in  $g\text{-C}_3\text{N}_4$  and  $\text{Bi/g-C}_3\text{N}_4\text{-HA-12}$  were examined. PL emissions of the samples under an excitation of 330 nm light were firstly measured, and **Fig. 3a** show that the PL spectra of both  $g\text{-C}_3\text{N}_4$  and  $\text{Bi/g-C}_3\text{N}_4\text{-HA-12}$  have two peaks centered at 439 and 468 nm due to the quantum confinement of  $g\text{-C}_3\text{N}_4$  nanosheets and the band-gap transition in  $g\text{-C}_3\text{N}_4$ , respectively [18]. The significant reduction in peak intensity of  $\text{Bi/g-C}_3\text{N}_4\text{-HA-12}$  suggests that  $e^-/h^+$  pair separation is significantly improved after the integration of Bi NPs. The improved  $e^-/h^+$  separation was further confirmed by the enlarged surface photovoltage response (SPV) in  $\text{Bi/g-C}_3\text{N}_4\text{-HA-12}$  compared to that in  $g\text{-C}_3\text{N}_4$  (See Fig. S5). All these demonstrate that Bi NPs actually work as the co-catalysts to promote  $e^-/h^+$  separation in  $g\text{-C}_3\text{N}_4$ , which should be responsible for the enhanced photocatalytic performance of  $\text{Bi/g-C}_3\text{N}_4$ .

In our system of  $\text{Bi/g-C}_3\text{N}_4$ ,  $g\text{-C}_3\text{N}_4$  is a well-known semiconductor photocatalyst with a visible-light-response band gap of 2.69 eV [12], while Bi NP is a plasmonic metal [26]. The synergistic interaction between Bi NPs and  $g\text{-C}_3\text{N}_4$  in photocatalysis could be schemed in **Fig. 3b**. Under illumination,  $e^-/h^+$  pairs are excited and dissociated within the semiconductor  $g\text{-C}_3\text{N}_4$ . Due to the intimate contact between Bi and  $g\text{-C}_3\text{N}_4$ , and the higher energy level of the conduction band edge of  $g\text{-C}_3\text{N}_4$  ( $-1.12$  eV) over the Fermi level of Bi NPs ( $-0.17$  eV), a metal-semiconductor heterojunction of  $\text{Bi-g-C}_3\text{N}_4$  will thus be constructed, and the excited  $e^-$  will spontaneously flow through the heterojunction from  $g\text{-C}_3\text{N}_4$  to Bi NPs. Bi NPs

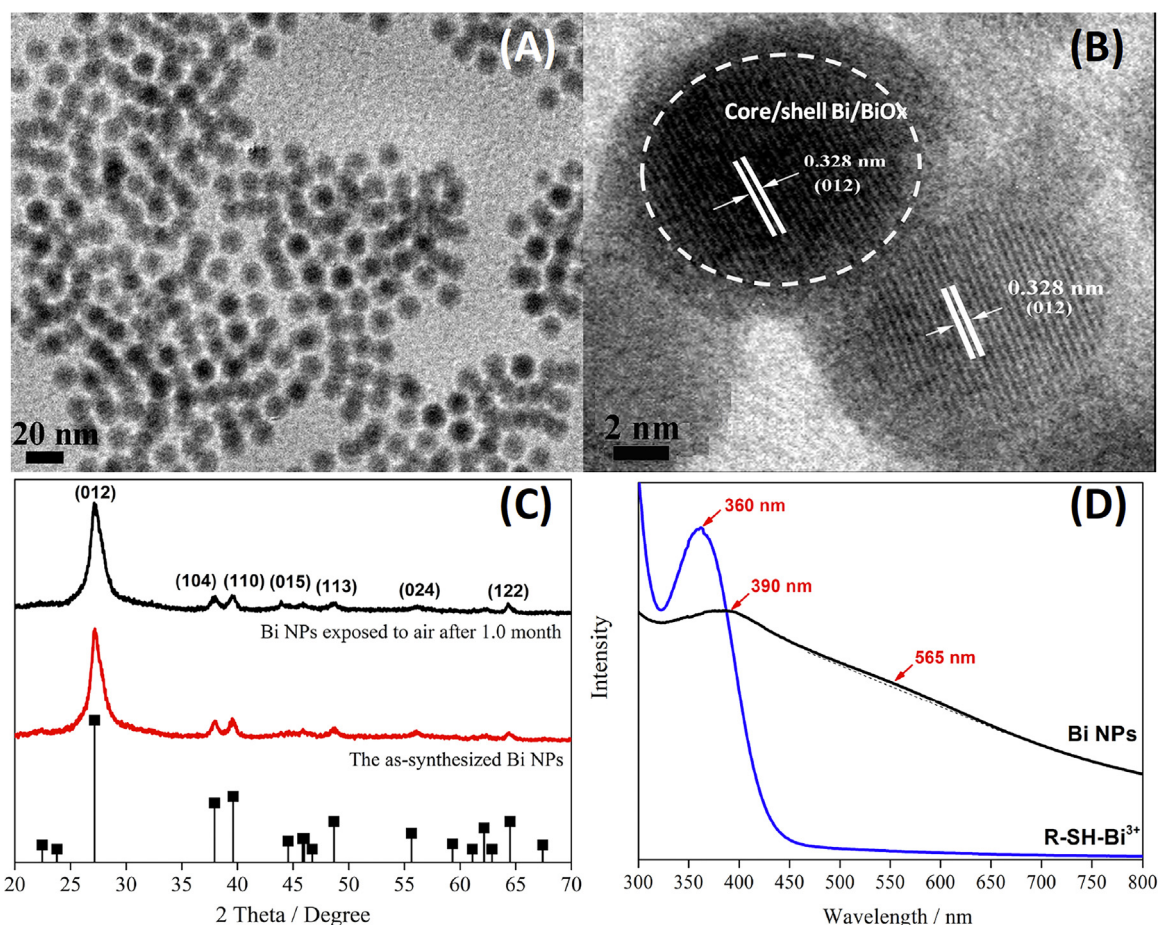


**Fig. 1.** TEM (A) and HRTEM (B) images of the as-synthesized Bi NPs; (C) XRD patterns of the as-synthesized Bi NPs and those after exposed to air for one month; (D) UV-vis spectra of  $\text{Bi}^{3+}$ -dodecanethiol ( $\text{R-SH-Bi}^{3+}$ ) precursor and the as-synthesized NPs dispersed in hexane.

serve as the electron “sink” and collect them for surface redox reactions. Unlike  $e^-$ , the separated  $h^+$  directly migrates to the surface of  $\text{g-C}_3\text{N}_4$  to initialize the oxidation reaction. Obviously, such a heterojunction effect can prevent  $e^-/h^+$  recombination in  $\text{g-C}_3\text{N}_4$  when a proper percentage of  $\text{Bi-g-C}_3\text{N}_4$  heterojunctions are formed. As a plasmonic metal, Bi NPs can concentrate incident photon energy into plasmon oscillations, and the concentrated resonance energy can be either transferred onto  $\text{g-C}_3\text{N}_4$  [27] or converted to a local electromagnetic field [28], both of which also facilitate  $e^-/h^+$  separation in  $\text{g-C}_3\text{N}_4$ . Accordingly, we can conclude that the superior promoting effect of Bi NPs on  $e^-/h^+$  separation is initiated by their two unique effects: (i) heterojunction effect and (ii) SPR effect.

### 3.3. Contribution identification for heterojunction effect and SPR effect

Though the role of Bi NP is unraveled and its promoting effect is also identified to arise from its heterojunction effect and SPR effect, the real contribution of each effect to photocatalysis is still unclear. The heterojunction effect depends much on Bi NP size. With a constant loading mass, depositing larger Bi NPs will produce a smaller number of heterojunctions and thus give a weak heterojunction effect. Accordingly, an increase in Bi NP size will lower the contribution of heterojunction effect. SPR effect is closely related to the plasmonic absorption ability of Bi NPs under illumination and the number of plasmonic units (i.e. the number of Bi NPs), both of which also rely much on their sizes [29]. In this work, Bi NPs with the sizes of  $7 \pm 0.5$ ,  $20 \pm 1.5$ ,  $50 \pm 2.5$  and  $80 \pm 2.5$  nm were successfully synthesized by simply adjusting the reaction temperature and the

concentration of reducing agent (the TEM images are presented in Fig. 4), and their SPR properties were characterized by UV-vis spectra. Fig. S6a show that with the size increasing from 7 to 80 nm, Bi NPs show a more and more intense absorption in the wavelength range of 300–800 nm, respectively. It indicates that larger Bi NPs have a stronger plasmonic absorption in visible light range, and are thus more likely to generate a stronger local electromagnetic field and a larger resonance energy acting on  $\text{g-C}_3\text{N}_4$ , and then an enhanced SPR effect. However, an increased Bi NP size will simultaneously decrease the number of plasmonic units, and weaken the SPR effect. Considering the close relationship of both the heterojunction and SPR effect with Bi NP size, we thus prepared a series of  $\text{Bi/g-C}_3\text{N}_4$  photocatalysts with Bi NPs of different sizes to tune the heterojunctions density and SPR intensity, and then compared their photocatalytic activities, which was expected to differentiate the contribution of each effect to the performance of  $\text{g-C}_3\text{N}_4$ .

Fig. S7 presents the TEM images of  $\text{Bi/g-C}_3\text{N}_4$ -HA composites with Bi NPs of different sizes. (7 nm Bi NPs decorated sample is denoted as  $\text{Bi/g-C}_3\text{N}_4$ -HA-7). 7 nm Bi NPs has the highest distribution density on  $\text{g-C}_3\text{N}_4$ , followed by 12, 20, 50 and 80 nm Bi NPs. The  $e^-/h^+$  separation efficiency and the photocatalytic activity of these  $\text{Bi/g-C}_3\text{N}_4$ -HA samples were then investigated. The PL spectra in Fig. 5a show that all  $\text{Bi/g-C}_3\text{N}_4$ -HA photocatalysts display lower intensities of emission peaks than  $\text{g-C}_3\text{N}_4$ , again confirming the promoting effect of Bi NPs on  $e^-/h^+$  separation. The same conclusion could be obtained from SPV results (See Fig. 5b), where a higher surface photovoltages on all  $\text{Bi/g-C}_3\text{N}_4$ -HA photocatalysts were detected over that in  $\text{g-C}_3\text{N}_4$ . Among  $\text{Bi/g-C}_3\text{N}_4$ -HA,  $\text{Bi/g-C}_3\text{N}_4$ -HA-12 shows the highest  $e^-/h^+$  separation efficiency with the lowest

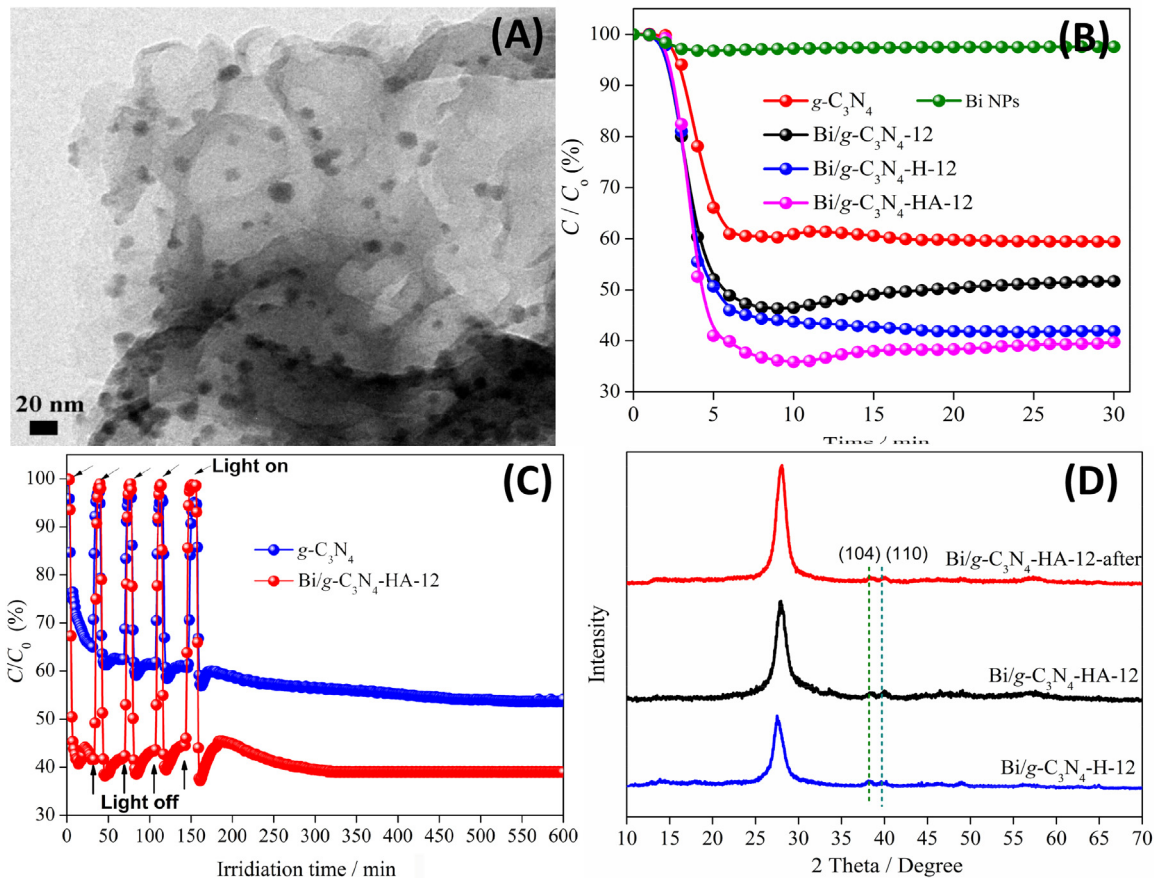


**Fig. 2.** (A) TEM image of Bi/g-C<sub>3</sub>N<sub>4</sub>-HA-12 photocatalyst; (B) Photocatalytic activities of the samples for NO removal in an air flow under visible light illumination (initial NO concentration: 500 ppb). (C) Durability test of the photocatalyst under the repeated on/off light conditions plus a long-term light illumination; (D) XRD patterns of Bi/g-C<sub>3</sub>N<sub>4</sub>-H as well as Bi/g-C<sub>3</sub>N<sub>4</sub>-HA before and after durability test.

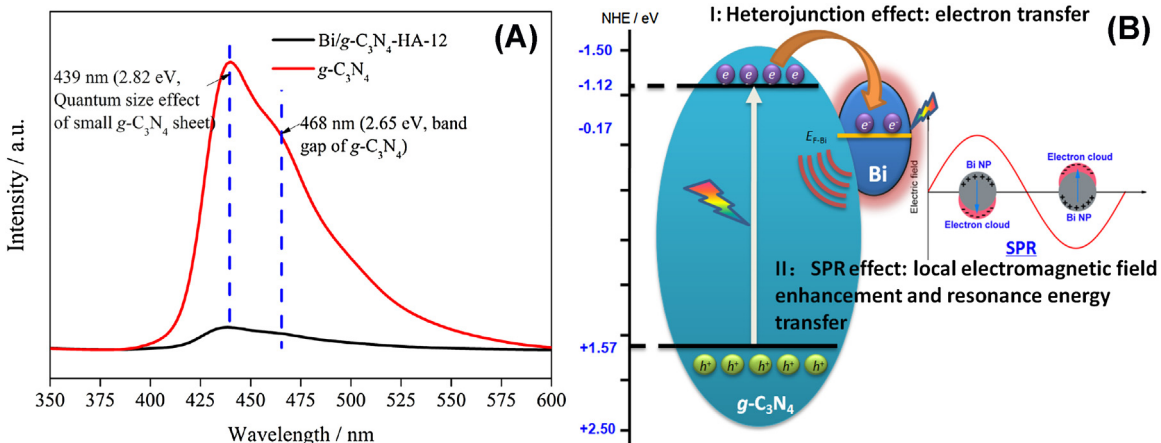


**Fig. 3.** (A) PL spectra of g-C<sub>3</sub>N<sub>4</sub> and Bi/g-C<sub>3</sub>N<sub>4</sub>-HA-12 under the excitation of 330 nm light; (B) Schematic process of the visible-light-response photocatalytic removal of NO on Bi/g-C<sub>3</sub>N<sub>4</sub> photocatalyst.

intensity of emission peak in PL spectrum and the largest surface photovoltage, followed by Bi/g-C<sub>3</sub>N<sub>4</sub>-HA-20, 7, 50 and 80. This order is interestingly consistent with that of their performances in photocatalytic removal of NO (Fig. 5c), where Bi/g-C<sub>3</sub>N<sub>4</sub>-HA-12 (a removal efficiency of 60.8%) performs over Bi/g-C<sub>3</sub>N<sub>4</sub>-HA-20 (54.8%), 7 (51.7%), 50 (48.1%) and 80 (42.3%). All the above confirm that  $e^-/h^+$  separation efficiency is the determining factor of photocatalytic activity in our system, and more importantly, demonstrate

a “volcano-like” variation of the photocatalytic activity of Bi/g-C<sub>3</sub>N<sub>4</sub>-HA versus Bi NP size.

The “volcano-like” variation of the photocatalytic activity of Bi/g-C<sub>3</sub>N<sub>4</sub>-HA versus Bi NP size should be ascribed to the synergy of size-dependent heterojunction effect and SPR effect of Bi NPs, which can be schemed in Fig. 5d. As demonstrated, an increase in Bi NP size will weaken the heterojunction and SPR effect by reducing the number of Bi-g-C<sub>3</sub>N<sub>4</sub> heterojunctions and plasmonic units, respectively, but in contrast, can enhance SPR effect by intensify-

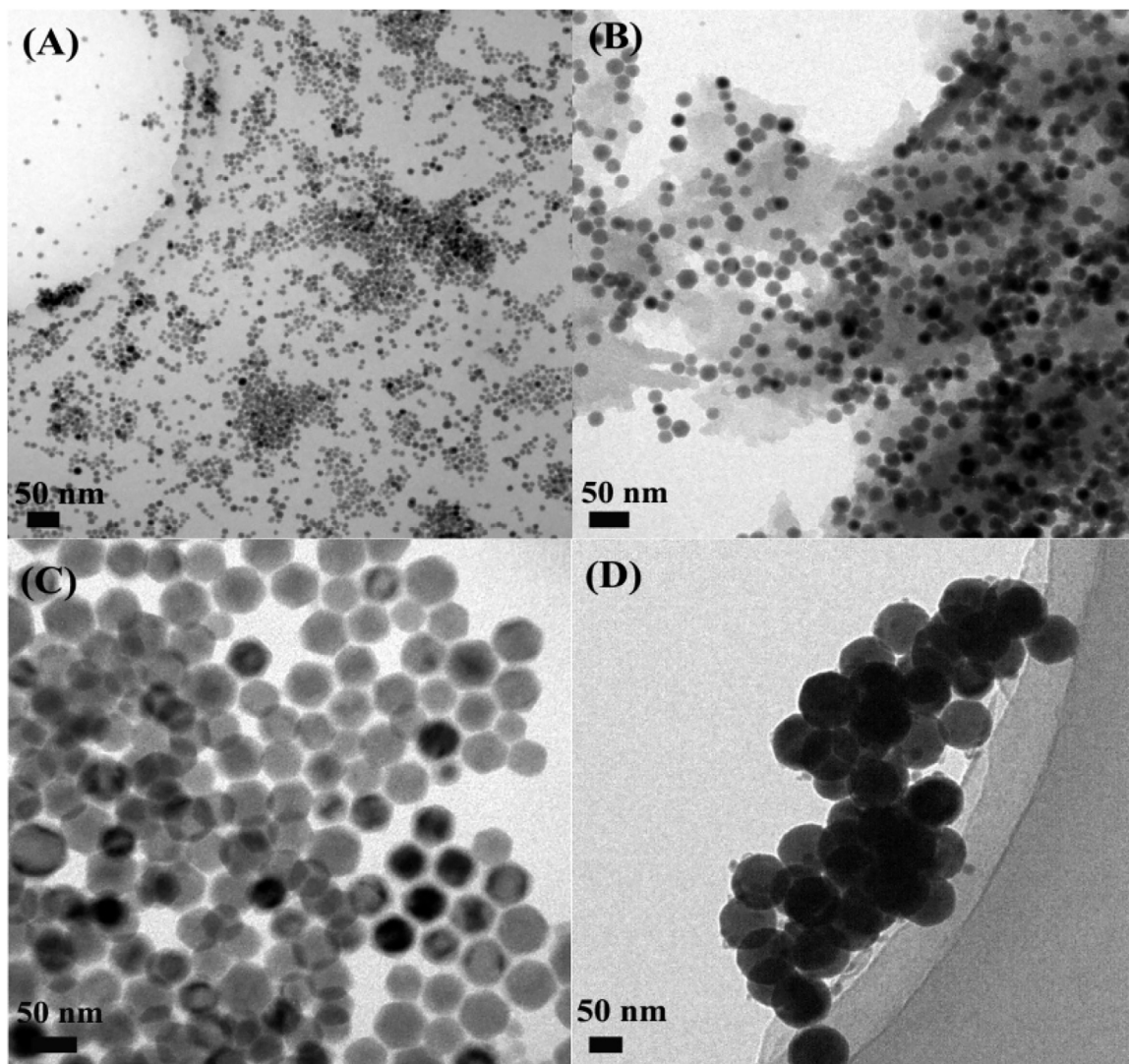


**Fig. 4.** TEM images of the as-synthesized Bi NPs with the sizes of 7 nm (A), 20 nm (B), 50 nm (C) and 80 nm (D).

ing plasmonic absorption. In the small size range (Bi size below the critical one), the enhanced photocatalytic activity with larger Bi NPs suggests that the SPR effect is strengthened in this region, and with Bi size increasing, the contribution of SPR effect rises faster than the contribution of heterojunction effect declines, rendering the overall contribution to go up. However, as Bi NP size is over a critical size, a further increase in Bi NP size will slow down the ascending of or even decrease the contribution of SPR effect due to the reduced amount of plasmonic units, and make it unable to catch up with the descending of the contribution of heterojunction effect, leading to a drop in overall contribution and then the photocatalytic activity. Accordingly, to maximize the synergy of SPR effect and heterojunction effect, a proper size of Bi NP has to be chosen, and in our system, 12 nm should be the nearly optimal Bi NP size.

Since the heterojunction density and the number of plasmonic units is also Bi mass-dependent, the photocatalytic activity could be further raised through optimizing the loading amount of Bi NPs. Fig. S8 shows that all Bi/g-C<sub>3</sub>N<sub>4</sub>-HA photocatalysts have a volcano-like activity deviation with Bi NP loading percentage. With increasing Bi amount, the quantity of the metal-semiconductor heterojunction and plasmonic unit increases, and thus an increased NO removal efficiency could be acquired (the ascending part of the curve). However, an over loading of Bi NPs will make the NPs cover more surface

area of g-C<sub>3</sub>N<sub>4</sub> to block light illumination, which will be detrimental to photocatalysis (the descending part in the curve). The optimal Bi loading varies with Bi NP size, and is around 32.1, 24.0, 21.4, 16.3 and 12.5 wt% for Bi/C<sub>3</sub>N<sub>4</sub>-HA-80, 50, 20, 12 and 7 nm, respectively.

### 3.4. Reaction pathway

For g-C<sub>3</sub>N<sub>4</sub>, the energy of the photoexcited  $e^-$  and  $h^+$  depends mainly on the band-edge positions of the conduction band and valence band of g-C<sub>3</sub>N<sub>4</sub>, lying theoretically at -1.12 and 1.57 eV, respectively. Under such a negative potential, the photoexcited  $e^-$  could reduce oxygen molecule ( $O_2$ ) in air into oxidative  $\bullet O_2^-$  radical (the redox potential for  $O_2$  into  $\bullet O_2^-$  is -0.33 eV), but not support the conversion of NO to  $N_2$  (the redox potential is -1.67 eV). The oxidative radical  $\bullet O_2^-$  could directly oxidize NO or get two more  $e^-$  transit into hydroxyl radical  $\bullet OH$  with the aid of water molecules, which is also an effective oxidant for NO oxidation. The  $h^+$  with the potential of 1.57 eV can directly oxidize NO, but could not trigger the generation of other oxidative radicals, such as the  $\bullet OH$  via the reaction  $h^+ + H_2O \rightarrow \bullet OH + H^+$  (1.99 eV). Accordingly, the oxidative radicals  $\bullet O_2^-$ ,  $\bullet OH$  and  $h^+$  are the potential agents those could remove NO. DMPO-ESR analyses were conducted on Bi/C<sub>3</sub>N<sub>4</sub>-HA-12, Bi NPs and g-C<sub>3</sub>N<sub>4</sub> to identify the active radicals and then explore more on the role of Bi NPs, and the results are

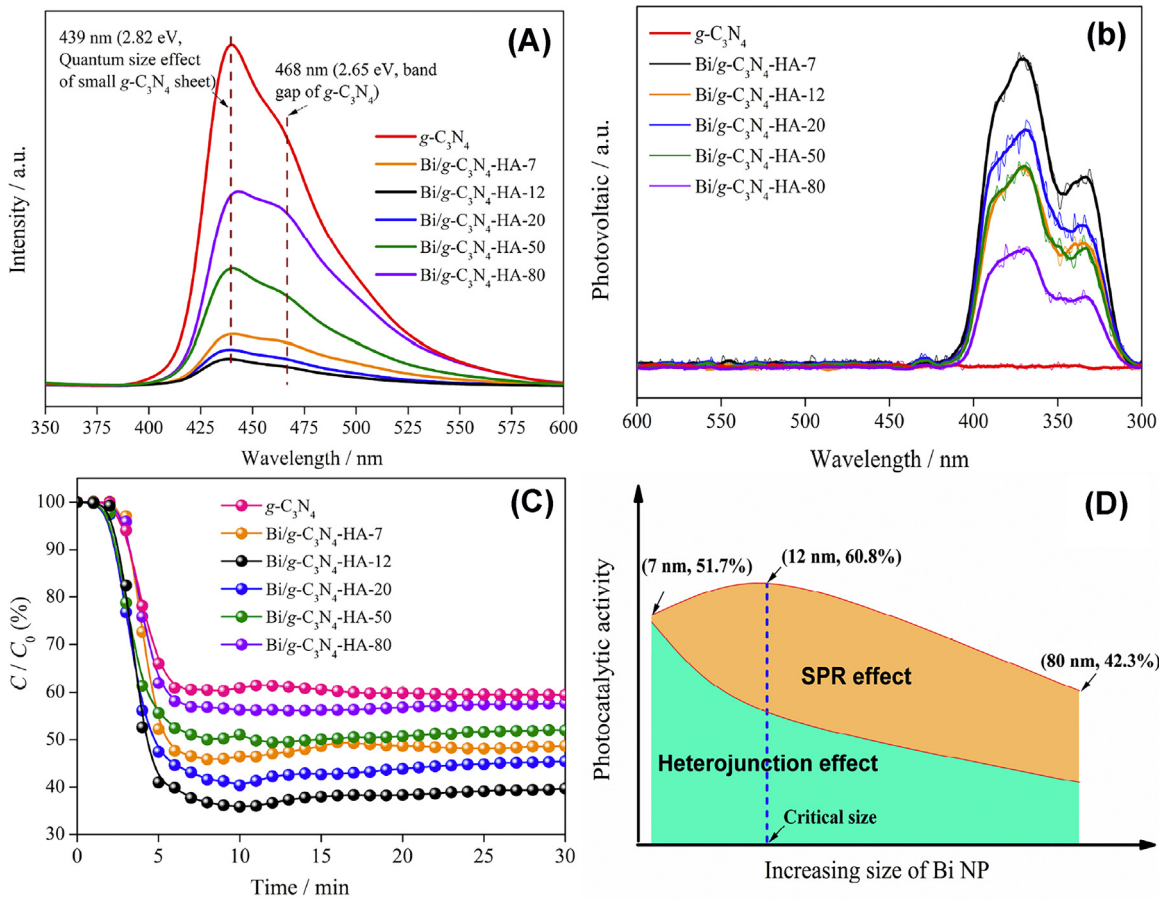


**Fig. 5.** PL spectra (A), the surface photovoltaic spectra(B) and photocatalytic activity (C) of the bare  $g\text{-C}_3\text{N}_4$  and the  $\text{Bi}/g\text{-C}_3\text{N}_4\text{-HA}$  with different Bi NP size (Bi loading of  $11.8 \pm 4$  wt%); (D) Schematic synergy of the size-dependent heterojunction effect and SPR effect of Bi NPs on the photocatalytic activity.

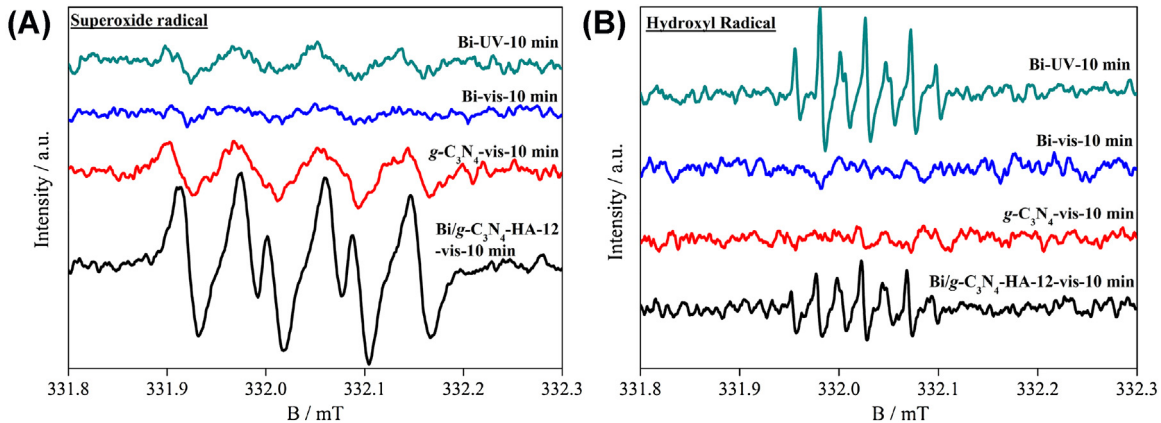


**Fig. 6.** DMPO spin-trapping spectra of Bi NPs,  $g\text{-C}_3\text{N}_4$  and  $\text{Bi}/\text{C}_3\text{N}_4\text{-HA-12}$  in methanol dispersion for  $\text{DMPO}\text{-}^{\bullet}\text{O}_2^-$  (A) and aqueous dispersion for  $\text{DMPO}\text{-}^{\bullet}\text{OH}$  (B).

presented in Fig. 6. On Bi NPs, the radicals including  $^{\bullet}\text{O}_2^-$  and  $^{\bullet}\text{OH}$  are only detected under UV illumination (280 nm) but not under visible light illumination, confirming the fact that the visible light is not energetic enough to produce  $^{\bullet}\text{O}_2^-$  and  $^{\bullet}\text{OH}$  on Bi NPs, consistent to the negligible NO removal efficiency of bare Bi NPs under visible light illumination. When comparing  $g\text{-C}_3\text{N}_4$  and  $\text{Bi}/\text{C}_3\text{N}_4\text{-HA-12}$ , it is found that the introduction of Bi NPs could not only enhance the yield of  $^{\bullet}\text{O}_2^-$ , but also trigger the generation of considerable amount of  $^{\bullet}\text{OH}$ . These results further demonstrate the importance of Bi NPs on photocatalytic removal of NO under visible light illumination.

To probe more into the photocatalytic NO oxidation process, *in situ* DRIFTS study was then performed on  $\text{Bi}/\text{C}_3\text{N}_4\text{-HA-12}$  with a mixed flow of NO and  $\text{O}_2$  under visible light illumination. Fig. 7 shows the IR spectra evolution along with the illumination time. At the zero time when NO adsorption-desorption reaches equilibrium, the bands at 974, 994, 1013, 1093, 1141, 1160 and 1176  $\text{cm}^{-1}$  were observed on IR spectrum (as indicated by the black dash line), all of which could be assigned to vibration of adsorbed NO on the surface of  $\text{Bi}/\text{C}_3\text{N}_4\text{-HA-12}$ , though its exact form and state ( $\text{N}_2\text{O}$ , NO or  $\text{NO}^-$ ) after the adsorption are unable to be identified. After the light illumination, the IR bands of NO at 974, 994 and 1013  $\text{cm}^{-1}$

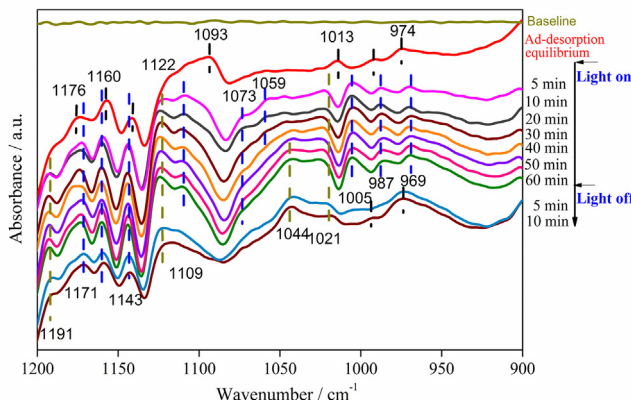


**Fig. 7.** *In situ* DRIFTS spectra analyses of the photocatalytic NO removal process on Bi/C<sub>3</sub>N<sub>4</sub>-HA-12 under a mixed flow of NO and O<sub>2</sub> with visible light illumination.

disappear totally, those at 1093 and 1176 cm<sup>-1</sup> display a reduced intensity, while those at 1140, 1160 and 1176 cm<sup>-1</sup> show a red-shift with the illumination time, all of which indicate that NO phase is undergoing oxidation. Along with the light illumination from 5 to 60 min, there appear some new bands locating at 969, 987, 1005, 1021, 1044, 1059, 1073, 1109, 1122, 1171 and 1191 cm<sup>-1</sup> with an increasing intensity on IR spectra. The bands at 969, 987, 1005 and 1059 cm<sup>-1</sup> refer to the vibration of the bridging nitrate and the bidentate nitrate (NO<sub>2</sub><sup>-</sup>), while those at 1021, 1044, 1073, 1109, 1122 and 1191 cm<sup>-1</sup> correspond to the vibration of the monodentate nitrate (NO<sub>3</sub><sup>-</sup>) [30]. The results suggest that NO are finally oxidized into bidentate or monodentate nitrate on Bi/C<sub>3</sub>N<sub>4</sub>-HA-12. When the light is turned off, the IR bands at 974, 994 and 1176 cm<sup>-1</sup> are recovered, those at 987, 1005 and 1109 cm<sup>-1</sup> gradually disappear, while those at 1021, 1044, 1122 and 1191 are preserved. Without the light illumination, no reactive radicals will be generated any more, which means that the transformation of NO to nitrate species will be stopped. The IR band variation after the light off, including the recovery, disappearance and preservation, thus corresponds to the re-sorption of NO phase, the desorption and accumulation of the products, respectively. All these suggest that NO will finally transform to bidentate/monodentate nitrate and accumulated on surface of Bi/C<sub>3</sub>N<sub>4</sub>-HA-12.

#### 4. Conclusions

In summary, we have presented a facile approach to the visible-light-response monodisperse Bi NPs-decorated g-C<sub>3</sub>N<sub>4</sub> photocatalyst, which is highly effective and durable for the removal of ppb-level NO in a continuous air flow at ambient condition. The decoration of Bi NPs could significantly enhance the performance of g-C<sub>3</sub>N<sub>4</sub>, and the enhancement arises from the heterojunction effect and SPR effect of Bi NPs. The contribution of heterojunction effect and SPR effect from Bi NPs is highly dependent on the size of Bi NPs, and by tuning the size of Bi NPs, an optimized synergy of these two effects could be achieved. On the catalyst surface, the photoexcited e<sup>-</sup> will transit into •O<sub>2</sub><sup>-</sup> and •OH, which serve as the leading radicals with h<sup>+</sup> participating in NO oxidation, and the NO will finally be converted to bidentate and monodentate nitrate and accumulated on surface of the photocatalyst. The work demonstrated here is expected to advance the application of the photocatalysis in real air purification.

#### Acknowledgements

The present work is financially supported by National Natural Science Foundation of China (Project 51508055, 51478070, 21501016), the National Key R&D Project of China (2016YFC0204702), and the Innovative Research Team of Chongqing (CXTDG201602014).

#### Appendix A. Supplementary data

Supplementary data associated with this article can be found, in the online version, at <http://dx.doi.org/10.1016/j.apcatb.2017.01.009>.

#### References

- [1] H. Akimoto, Global air quality and pollution, *Science* 302 (2003) 1716–1719.
- [2] A.M. Fiore, V. Naik, D.V. Spracklen, A. Steiner, N. Unger, M. Prather, D. Bergmann, P.J. Cameron-Smith, I. Cionni, W.J. Collins, S. Dalsoren, V. Eyring, G.A. Folberth, P. Ginoux, L.W. Horowitz, B. Josse, J.F. Lamarque, I.A. Mackenzie, T. Nagashima, F.M. O'Connor, M. Righi, S.T. Rumbold, D.T. Shindell, R.B. Skeie, K. Sudo, S. Szopa, T. Takemura, G. Zeng, Global air quality and climate, *Chem. Soc. Rev.* 41 (2012) 6663–6683.
- [3] F. Rezaei, A.A. Rownagh, S. Monjezi, R.P. Lively, C.W. Jones, SO<sub>x</sub>/NO<sub>x</sub> removal from flue gas streams by solid adsorbents: a review of current challenges and future directions, *Energ. Fuel* 29 (2015) 5467–5486.
- [4] S.G. Xiong, J.X. Weng, Y. Liao, B. Li, S.J. Zou, Y. Geng, X. Xiao, N. Huang, S.J. Yang, Alkali metal deactivation on the low temperature selective catalytic reduction of NO<sub>x</sub> with NH<sub>3</sub> over MnO<sub>x</sub>-CeO<sub>2</sub>: a mechanism study, *J. Phys. Chem. C* 120 (2016) 15299–15309.
- [5] A. Wang, Y.L. Guo, F. Gao, C.H.F. Peden, Ambient-temperature NO oxidation over amorphous CrO<sub>x</sub>-ZrO<sub>2</sub> mixed oxide catalysts: significant promoting effect of ZrO<sub>2</sub>, *Appl. Catal. B: Environ.* (2016), <http://dx.doi.org/10.1016/j.apcatb.2016.02.045>.
- [6] R. Asahi, T. Morikawa, T. Ohwaki, K. Aoki, Y. Taga, Visible-light photocatalysis in nitrogen-doped titanium oxides, *Science* 293 (2001) 269–271.
- [7] R. Asahi, T. Morikawa, H. Irie, T. Ohwaki, Nitrogen-doped titanium dioxide as visible-light-sensitive photocatalyst: designs, developments, and prospects, *Chem. Rev.* 114 (2014) 9824–9852.
- [8] X.F. Ning, S.G. Meng, X.L. Fu, X.J. Ye, S.F. Chen, Efficient utilization of photogenerated electrons and holes for photocatalytic selective organic syntheses in one reaction system using a narrow band gap CdS photocatalyst, *Green Chem.* 18 (2016) 3628–3639.
- [9] C. Pan, J. Xu, Y. Wang, D. Li, Y. Zhu, Dramatic activity of C<sub>3</sub>N<sub>4</sub>/BiPO<sub>4</sub> photocatalyst with core/shell structure formed by self-assembly, *Adv. Funct. Mater.* 22 (2012) 1518–1524.
- [10] F. Dong, W.K. Ho, S.C. Lee, Z.B. Wu, M. Fu, S.C. Zou, Y. Huang, Template-free fabrication and growth mechanism of uniform (BiO)<sub>2</sub>CO<sub>3</sub> hierarchical hollow microspheres with outstanding photocatalytic activities under both UV and visible light irradiation, *J. Mater. Chem. A* 21 (2011) 12428–12436.
- [11] R. Kuriki, K. Sekizawa, O. Ishitani, K. Maeda, Visible-light-driven CO<sub>2</sub> reduction with carbon nitride: enhancing the activity of ruthenium catalysts, *Angew. Chem. Int. Ed.* 54 (2015) 2406–2409.
- [12] X.C. Wang, K. Maeda, A. Thomas, K. Takanabe, G. Xin, J.M. Carlsson, K. Domen, M. Antonietti, A metal-free polymeric photocatalyst for hydrogen production from water under visible light, *Nat. Mater.* 8 (2009) 76–80.
- [13] Y. Zheng, J. Liu, J. Liang, M. Jaroniec, S.Z. Qiao, Graphitic carbon nitride materials: controllable synthesis and applications in fuel cells and photocatalysis, *Energy Environ. Sci.* 5 (2012) 6717–6731.
- [14] Z. Zhao, Y. Sun, F. Dong, Graphitic carbon nitride based nanocomposites: a review, *Nanoscale* 7 (2015) 15–37.
- [15] P. Niu, L.L. Zhang, G. Liu, H.M. Cheng, Graphene-like carbon nitride nanosheets for improved photocatalytic activities, *Adv. Funct. Mater.* 22 (2012) 4763–4770.
- [16] F. Dong, Z.Y. Wang, Y.H. Li, W.K. Ho, S.C. Lee, Immobilization of polymeric g-C<sub>3</sub>N<sub>4</sub> on structured ceramic foam for efficient visible light photocatalytic air purification with real indoor illumination, *Environ. Sci. Technol.* 48 (2014) 10345–10353.
- [17] S.W. Zhang, J.X. Li, X.K. Wang, Y.S. Huang, M. Zeng, J.Z. Xu, In situ ion exchange synthesis of strongly coupled Ag@AgCl/g-C<sub>3</sub>N<sub>4</sub> porous nanosheets as plasmonic photocatalyst for highly efficient visible-light photocatalysis, *ACS Appl. Mater. Interfaces* 6 (2014) 22116–22125.
- [18] F. Dong, Z.W. Zhao, Y.J. Sun, Y.X. Zhang, S. Yan, Z.B. Wu, An advanced semimetal-organic Bi spheres-g-C<sub>3</sub>N<sub>4</sub> nanohybrid with SPR-enhanced visible-light photocatalytic performance for NO purification, *Environ. Sci. Technol.* 49 (2015) 12432–12440.
- [19] J.S. Son, K. Park, M.K. Han, C. Kang, S.G. Park, J.H. Kim, W. Kim, S.J. Kim, T. Hyeon, Large-scale synthesis and characterization of the size-dependent thermoelectric properties of uniformly sized bismuth nanocrystals, *Angew. Chem. Int. Ed.* 50 (2011) 1363–1366.

[20] F. Dong, L.W. Wu, Y.J. Sun, M. Fu, Z.B. Wu, S.C. Lee, Efficient synthesis of polymeric g-C<sub>3</sub>N<sub>4</sub> layered materials as novel efficient visible light driven photocatalysts, *J. Mater. Chem.* 21 (2011) 15171–15174.

[21] Y. Zhou, Z.Y. Zhao, F. Wang, K. Cao, D.E. Doronkin, F. Dong, J.D. Grunwaldt, Facile synthesis of surface N-doped Facile synthesis of surface N-doped Bi<sub>2</sub>O<sub>2</sub>CO<sub>3</sub>: origin of visible light photocatalytic activity and in situ DRIFTS studies, *J. Hazard. Mater.* 307 (2016) 163–172.

[22] Z.Y. Zhang, M.F. Chi, G.M. Veith, P.F. Zhang, D.A. Lutterman, J. Rosenthal, S.H. Overbury, S. Dai, H.Y. Zhu, Rational design of Bi nanoparticles for efficient electrochemical CO<sub>2</sub> reduction: the elucidation of size and surface condition effects, *ACS Catal.* 6 (2016) 6255–6264.

[23] S. Zhang, G.M. Jiang, G.T. Filsinger, L.H. Wu, H.Y. Zhu, J. Lee, Z.B. Wu, S.H. Sun, Halide ion-mediated growth of single crystalline Fe nanoparticles, *Nanoscale* 6 (2014) 4852–4856.

[24] Z. Wang, C.L. Jiang, R. Huang, H. Peng, X.D. Tang, Investigation of optical and photocatalytic properties of bismuth nanospheres prepared by a facile thermolysis method, *J. Phys. Chem. C* 118 (2014) 1155–1160.

[25] M. Cargnello, V.V. Doan-Nguyen, T.R. Gordon, R.E. Diaz, E.A. Stach, R.J. Gorte, P. Fornasiero, C.B. Murray, Control of metal nanocrystal size reveals metal-support interface role for ceria catalysts, *Science* 341 (2013) 771–773.

[26] F. Dong, T. Xiong, Y.J. Sun, Z.W. Zhao, Y. Zhou, X. Feng, Z.B. Wu, A semimetal bismuth element as a direct plasmonic photocatalyst, *Chem. Commun.* 50 (2014) 10386–10389.

[27] S.K. Cushing, J. Li, F. Meng, T.R. Senty, S. Suri, M. Zhi, M. Li, A.D. Bristow, N. Wu, Photocatalytic activity enhanced by plasmonic resonant energy transfer from metal to semiconductor, *J. Am. Chem. Soc.* 134 (2012) 15033–15041.

[28] T. Xiong, X. Dong, H.W. Huang, W.L. Cen, Y.X. Zhang, F. Dong, Single precursor mediated-synthesis of Bi semimetal deposited N-doped (BiO)<sub>2</sub>CO<sub>3</sub> superstructures for highly promoted photocatalysis, *ACS Sustain. Chem. Eng.* 4 (2016) 2969–2979.

[29] J. Touderet, R. Serna, M.J. Castro, Exploring the optical potential of nano-bismuth: tunable surface plasmon resonances in the near ultraviolet-to-near infrared range, *J. Phys. Chem. C* 116 (2012) 20530–20539.

[30] K. Hadjiivanov, V. Avreyska, D. Klissurski, T. Marinova, Surface species formed after NO Adsorption and NO + O<sub>2</sub> coadsorption on ZrO<sub>2</sub> and sulfated ZrO<sub>2</sub>: an FTIR spectroscopic study, *Langmuir* 18 (2002) 1619–1625.